Laser-Doppler measurement of crosswind velocity

F. Durst, B. M. Howe, and G. Richter

There is a need for the remote sensing of local wind velocities over distances of hundreds of meters, and laser-Doppler anemometry (LDA) has been suggested as a suitable measuring technique. In this paper the major features of an LDA system optimized for crosswind velocity measurements are presented. Computer programs based on Mie scattering theory are used to predict the performance of such systems and to extend the experimentally verified information to larger distances. A complete system for the measurement of the crosswind velocity component is described, and measurements up to 106 m verifying its performance and corresponding predictions are presented and discussed. Suggestions for further studies and developments are given.

I. Introduction

A. General

During the last decade intensive research has been carried out in the field of laser-Doppler anemometry (LDA) resulting in instruments that can be employed to make nonintrusive measurements of local fluid flow velocity in laboratory flow situations. The success of LDA in different fields of science and engineering initiated research and development to extend the measuring technique to long distances in general and wind velocity measurements in particular. Research efforts have aimed at complete LDA systems capable of measuring wind velocities at various points in the atmosphere up to distances of 1000 m and more. Such measurements would yield data useful in such fields as meteorology, wind energy, planetary boundary layer and atmospheric turbulence studies, military applications, etc. Detailed studies of wind fields would be possible with scanning laser-Doppler systems, providing more information over larger spatial regions, more quickly, and at lower cost than with conventional instruments, which usually require measuring towers, balloons, etc. LDA systems for wind velocity measurements over large distances are not readily available yet, and more work is needed to set up functioning instruments for three component wind velocity measurements. This paper summarizes work of this kind carried out by the authors to provide a basis for the installation of an LDA system for remote sensing of crosswind fields. It is the measurement of crosswind components over large distances that has not been dealt with in the literature.

The authors' research and development efforts in LDA wind velocity measurements took into account the existing information mainly relating to measurements of the vertical wind field by means of CO_2 reference-beam anemometers, e.g., see Refs. 1–16. Crosswind measurements using visible radiation have been attempted in the past, but no practical measurements have yet been made. This is also reflected by the literature survey carried out prior to this work. From it the following conclusions can be drawn:

(a) The research and development in the field of CO_2 wind velocity measuring systems are far advanced. Applicable instruments are available and have been successfully used for measurements over large distances, showing good agreement with conventional velocity measuring instruments.

(b) Research and development on long-range dual-beam anemometry are less advanced. Attempts to measure the velocity components perpendicular to the axis of the transmission optics have been undertaken using visible laser radiation. Only a few actual measurements of the cross-axial velocity components exist and these only over relatively small distances.

(c) There is a need for remote measurements of 3-D wind velocities. Optimum optical systems are likely to incorporate a CO_2 reference-beam system for the axial velocity component and dual-beam systems using visible laser radiation to measure the cross-axial velocity components.

The authors are with Universität Karlsruhe, Abteilung III: Mechanik Turbulenter Strömungen, Institut für Hydromechanik, 7500 Karlsruhe 1, Postfach 6380, Federal Republic of Germany.

Received 22 May 1981.
0003-6935/82/142596-12$01.00/0.

(d) Further research and development are needed to deepen the existing knowledge of such systems. Theoretical and experimental information is far less advanced for the measurement of crosswind velocity components.

The above conclusions were taken into account in the authors' research and development, which aimed at an advancement of the existing knowledge on laser-Doppler measurements of wind fields and at the development of a working system capable of measuring over several hundred meters. General requirements to ensure the functioning of such a system are given in Sec. II, where the employment of computer programs is described to predict the resultant signal strength as a function of the optical system, the laser power, the measuring distance, and particle properties. It is shown that photon-resolved signals need to be detected for long-distance LDA measurements. Such signals require special processing systems summarized in Sec. III. Section IV describes a complete single-channel laser-Doppler system set up at the Universität Karlsruhe for wind velocity measurements. Details of the optical system are given and its performance for wind velocity measurements at various distances is demonstrated. Comparisons with a sonic anemometer are described. Data that demonstrate the satisfactory performance of the system are given, and suggestions for further investigations and developments are provided. Conclusions and final remarks are given in Sec. V.

B. Nomenclature

A_j elements of detector area,
$C(r_p)$ concentration of aerosols of radius r_p,
f_D Doppler frequency,
G normalized scattered intensity,
$G(\tau)$ correlation function,
h Planck's constant,
k wave vector $(2\pi/\lambda)$,
m refractive index of particle material,
m_v Michelson fringe visibility,
$\dot{N}_e$ electron pulse rate,
$\dot{N}_{ph}$ photon rate,
N_c number of correlator channels,
P_L laser power,
P_s light power scattered by spherical particles,
$P_u(u)$ velocity probability distribution,
R distance between scattering particles and detector center,
R_D radius of detector area,
r_p radius of scattering particle,
r_{ij} distance between scattering particle and center of detector area element,
s radius of measuring volume,
T transmission of optical bandpass filter,
t time,
t_i arrival time of particle i,
U_i velocity components,
V crosswind velocity,
$\Gamma(\theta,\phi)$ Mie scattering function,
η_i modulation depth of LDA signal,

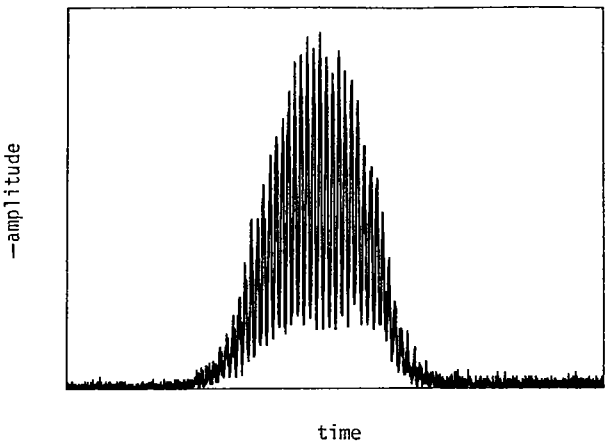

Fig. 1. Laser-Doppler signal for high ratios of electron pulse rate to Doppler frequency.

η_q quantum efficiency of PM tube,
$\Delta\tau_i$ transit time of particle i through the measuring volume,
τ correlation lag time, and
ν light frequency.

II. Signal Detectability and Aerosol Properties

The application of laser-Doppler anemometers to fluid velocity measurements is dependent on the presence of suitable scattering particles. Their passage through the measuring volume results in optical signals with an instantaneous scattered light power given by the following expression:

$$P_s = \sum_{i=1}^{N} (P_s)_i = \sum_{i=1}^{N} (P_s)_{o,i} \cdot \exp\left[-\frac{(t-t_i)^2}{\Delta\tau_i^2}\right] \{1 + \eta_i \cos[2\pi f_{D,i}(t-t_i)]\}, \quad (1)$$

where $(P_s)_i$ is the scattered light power detected from the ith particle. The quantity $(P_s)_{o,i}$ is dependent on the local light intensity in the center of the measuring volume and, therefore, on the applied laser power and focusing properties of the transmission optics.

In a conventional laser-Doppler system the scattered light power [analytically described by Eq. (1)] is detected by a photomultiplier which converts $\dot{N}_{ph}$ photons per second into $\dot{N}_e$ electron pulses per second:

$$\dot{N}_e = \eta_q \dot{N}_{ph} = \frac{P_s}{h \cdot \nu} \eta_q = \sum_{i=1}^{N} \eta_q \frac{(P_s)_{o,i}}{h \cdot \nu} \exp\left[-\frac{(t-t_i)^2}{\Delta\tau_i^2}\right] \{1 + \eta_i \cos[2\pi f_{D,i}(t-t_i)]\}. \quad (2)$$

These electron pulses are received at the anode of the photomultiplier. If the ratio of electron pulse rate $\dot{N}_e$ to Doppler frequency f_D is high, the number of electron pulses that are summed up to give the amplitude of the Doppler signal is high and continuous signals as shown in Fig. 1 result. However, if the ratio $(\dot{N}_e/f_D)$ is small, the resultant signal at the anode will consist of individual electron pulses as schematically shown in Fig. 2. Signals of this kind result from laser-Doppler anemometers when applied over long distances. Although these signals consist of individual electron pulses, the variation of the pulse rate is still described by Eq. (2).

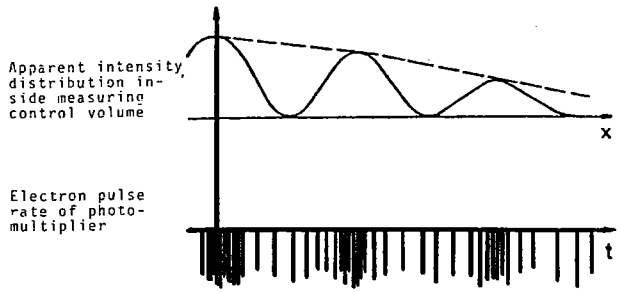

Fig. 2. Laser-Doppler signal for low ratios of electron pulse rate to Doppler frequency.

This figure indicates that the pulse rate shows maxima and minima in time intervals corresponding to the time of flight of the scattering particles between two intensity maxima or minima in the apparent fringe pattern in the measuring volume. Hence the time of flight needed to compute the velocity information can still be deduced as the time between the maxima or minima of the detected electron pulse rates. To ensure the detectability of the Doppler frequency the ratio of the electron pulse rate to the Doppler frequency at the anode of the photomultiplier has to exceed 1, at least in the center of the measuring volume, e.g.,

$$\frac{(\dot{N}_e)_o}{f_D} = \frac{\eta_q (P_s)_{o,i}}{h \cdot \nu \cdot f_D} = \frac{P_L \cdot G_i \cdot \eta_q}{\pi \cdot s^2 \cdot k^2 \cdot h \cdot \nu \cdot f_D} \gtrsim 1. \tag{3}$$

This pulse rate ensures that more than one electron pulse per Doppler cycle results from one particle at least in the center of the measuring volume. The equation shows that the pulse rate is dependent on the incident laser power P_L, the wavelength of the applied laser radiation λ, e.g. on $k = 2\pi/\lambda$, the measuring volume radius s, the integrated normalized scattered intensity G_i, and the Doppler frequency f_D. With increasing Doppler frequency the light power must be increased to ensure signal detectability if all the remaining influencing factors are constant.

The above formulas allow the following quantities to be computed, as an example, for LDA signals with Doppler frequencies $f_D = 100$ kHz. For such signals an electron pulse rate of $\dot{N}_e \geq 10^5\ \text{sec}^{-1}$ is needed from the center of the measuring volume. With a 12-Å bandwidth filter and transmission $T = 0.5$, a photomultiplier quantum efficiency of $\eta_q = 0.2$, and a laser wavelength of $\lambda = 514.5$ nm, the average scattered power has to exceed

$$(P_s)_0 \geq 3.8 \times 10^{-13}\ \text{W} \tag{4}$$

for a single particle. Higher powers lead to good detectable signals, whereas lower powers do not add constructively to the correlator signal but act as statistical background noise.

With the help of a computer program, see Ref. 17, the light power scattered by single spherical particles passing through the measuring control volume can be calculated. This program, based on Mie scattering theory[18] takes into account the light intensity distribution in the measuring volume, the wavelength of incident laser radiation, and properties of the detection system. The detectable scattered power P_s is a function of the particle radius r_p, the complex refractive index m of the particle material, the laser wavelength λ and laser power P_L, the distance between scattering center and detector R, and the detector radius R_D.

Because of the occurrence of scattering lobes in space, accurate computation of the scattered light power P_s requires the detector area to be subdivided into several detector elements, and the light power impinging onto each element has to be computed separately:

$$P_s = P_L \frac{1}{\pi s^2} \int_A \frac{1}{r_{ij}^2} \Gamma_{ij}(\theta,\phi) dA_j, \tag{5}$$

where $\Gamma_{ij}(\theta,\phi)$ = Mie scattering function,
dA_j = elements of detector area, and
r_{ij} = distance between scattering particles and center of detector area element.

Equation (5) shows that the received scattered power is proportional to the laser power P_L and, with certain restrictions, to the detector area $A = \Sigma A_j$ ($= \pi R_D^2$ for circular apertures). The influence of the scattering particles is embodied in $\Gamma_{ij}(\theta,\phi)$. This quantity depends on particle size given by the radius r_p and the complex refractive index m, of which the imaginary part represents the absorption.

LDA measurements of local wind velocity over large distances rely entirely on the availability of natural scattering particles, i.e., on aerosols. As shown in the literature, e.g., see Ref. 19, their size distribution, their concentration, and the optical properties of the particle material vary widely and are dependent, among other influencing factors, on regional aerosol sources and weather conditions. Despite these wide variations and dependence on many influencing factors, attempts have been made to categorize particles into the groups maritime, rural, and urban. These groups of aerosol show large variations in the refractive index of the particle material, yielding large differences in scattered light power.

These differences are apparent from Figs. 3(a)–(c), which show computed light powers as a function of particle size and for three different refractive indices corresponding to the average value of each of the above groups of particles. Taking into account the derived detection limit for the Doppler frequency, Figs. 3(a)–(c) indicate that only particles with diameters in excess of (a) maritime: $d_p \geq 0.7\ \mu$m, (b) rural: $d_p \geq 0.7\ \mu$m, and (c) urban: $d_p \geq 2.0\ \mu$m scatter sufficient light to permit laser-Doppler measurements. These results were computed for a measuring distance of 100 m, and the optical system described in Sec. IV.

III. Signal Processing and Data Analysis

For LDA wind velocity measurements the signal at the output of the photomultiplier consists of individual electron pulses produced by individual photons at the cathode and amplified by secondary electron emission in the dynode chain of the photomultiplier. In the present study these pulses were processed by a discriminator–amplifier to yield rectangular pulses of

constant height and 50-nsec width. These regular pulses were fed to the input of a 50-nsec 72-channel (K7023 Malvern Instruments) digital correlator to obtain the autocorrelation of the arriving pulse train. The correlator was operated in the single clip mode providing an autocorrelation function close to the unclipped form, see Ref. 20. A Hewlett-Packard 21 MX mini-

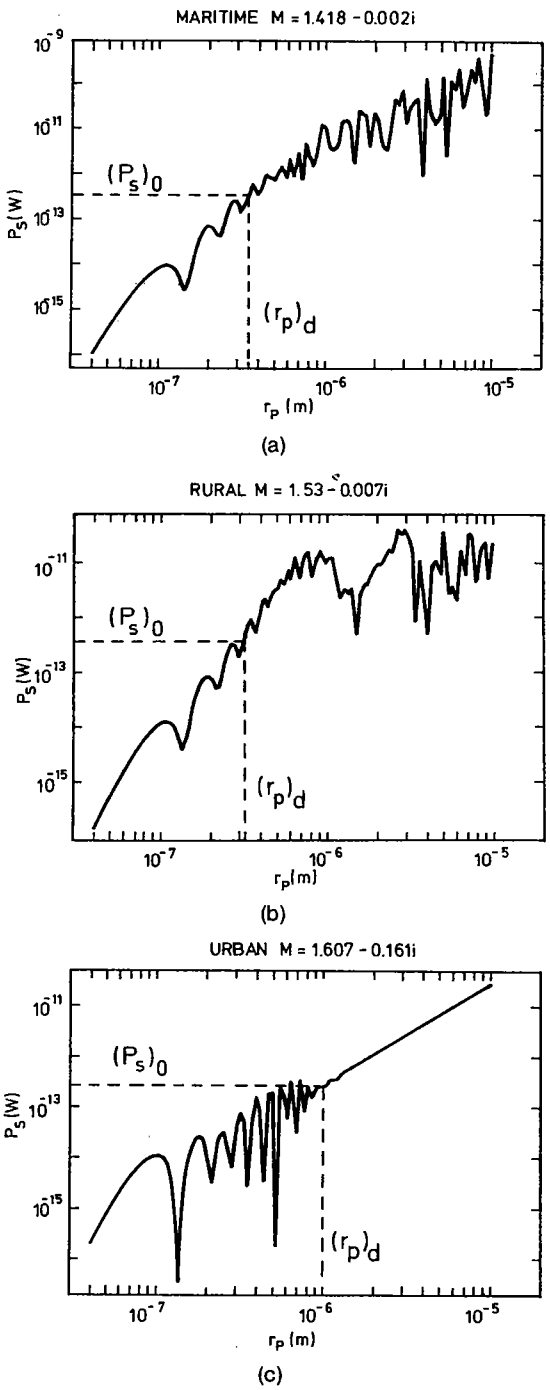

Fig. 3. Influence of particle size and refractive indices on scattered light power (λ = 514.5 nm): (a) maritime aerosol m = 1.418–0.002i; (b) rural aerosol m = 1.53–0.007i; and (c) urban aerosol m = 1.607–0.161i. $(P_s)_o$ = Minimum light power required for signal detectability; $(r_p)_d$ = minimum particle radius to produce detectable signals.

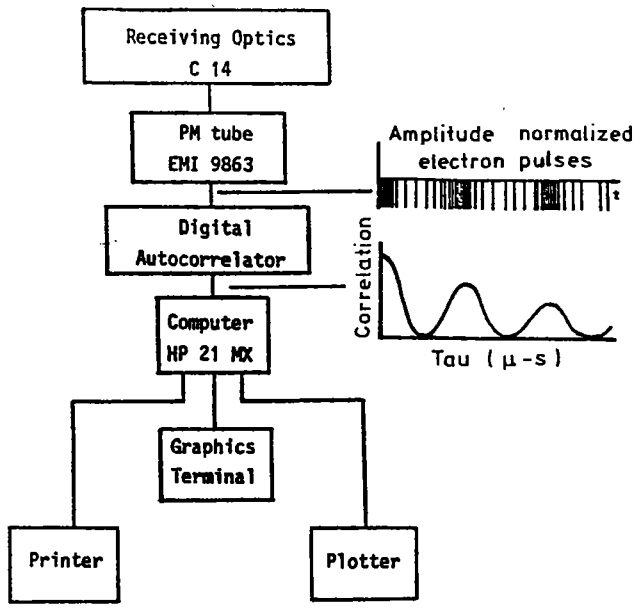

Fig. 4. Block diagram of signal processing electronics.

computer was employed to read and process the autocorrelations, to control the data acquisition, and to perform subsequent data analysis. A block diagram of the complete electronic system is shown in Fig. 4. To understand its functioning details of the signal treatment are provided below.

It has been shown[21] that the autocorrelation function of the pulse train of Fig. 2 can be described for simple ideal cases as a modulated damped Gaussian function; see also Eq. (2). The frequency content of this function and its shape can be explained by particles successively crossing bright and dark fringes that can be thought of as being located in the measuring control volume. The probability of a photon being emitted is high while the particles are in the region of bright fringes but is less when they are in regions of dark fringes. The amount of damping of the resultant autocorrelation function is related to the measuring volume dimensions, the light intensity distribution in the volume, and the velocity variations between particles within the correlation integration time. With the assumption that the beam profile is Gaussian in the measuring volume and the rms value of the signal frequency variation is <15%, the correlation function is given by

$$G(\tau) = A \cdot \exp\left[\left(-\frac{\tau}{\Delta\tau_i}\right)^2\right] \int_{-\infty}^{+\infty} P_u(u) \cdot \left(1 + \frac{m_v^2}{2} \cos\frac{2\pi u\tau}{\Delta x}\right) du + B. \tag{6}$$

Here τ is the correlation lag time, $\Delta\tau_i$ is a measure of the transit time of the particles through the measuring volume, Δx is the fringe spacing, A is the amplitude of the resultant signal, and B is the part of the autocorrelation which corresponds to the background dc level of the incoming light. The entire problem in the analysis is to extract $P_u(u)$, the velocity probability distribution, or at least the first or second moments. (Basic references presenting the above function are 20 and 21.)

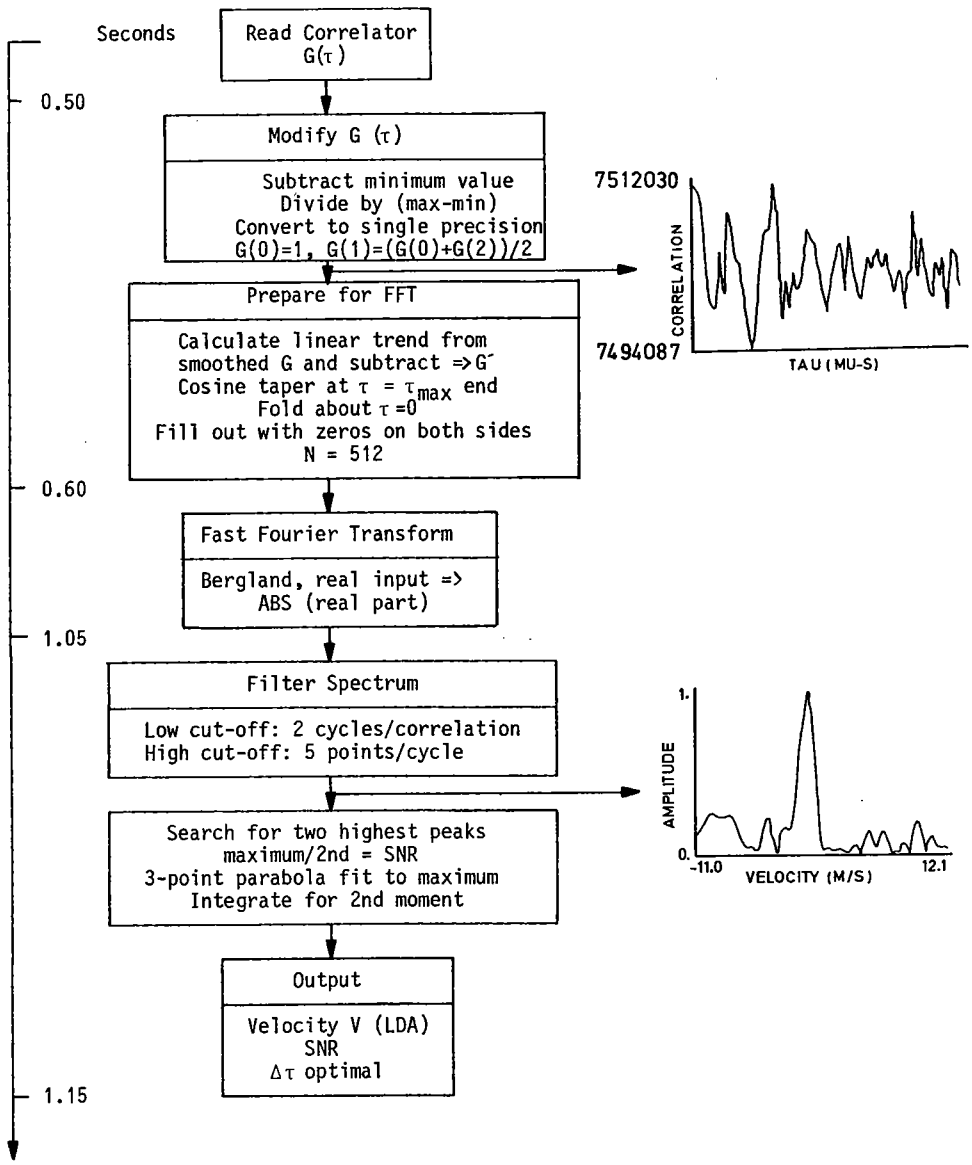

Fig. 5. Flow chart providing information on computational steps.

Making the assumption that $N_c \cdot \tau \geq \Delta\tau_i$ (a good one in practice), the exponential term can be approximated by unity. (This corresponds to the approximation of a Gaussian curve by a straight line in the center part of the curve.) Using the definition

$$\int_{-\infty}^{+\infty} P_u(u)du = 1,$$

and stipulating that all velocities relative to the fringe system are positive (frequency shifting is probably necessary), on rearranging gives

$$G'(\tau) = \frac{G(\tau) - A - B}{A \cdot m_0^2/2} = \int_0^{\infty} P(u) \cos\left(\frac{2\pi u\tau}{\Delta x}\right) du. \qquad (7)$$

This equation can be recognized as one-half of a cosine transform pair, the inverse transformation being

$$P_u(u) = \int_0^{\infty} G'(\tau) \cdot \cos\left(\frac{2\pi u\tau}{\Delta x}\right) du. \qquad (8)$$

Thus, by using a cosine transform or equivalent, in this work a fast Fourier transform (FFT), one can obtain $P_u(u)$, and from this obtain the desired velocity information.

A flow chart describing the actual computational steps taken by the authors in analyzing the autocorrelation is given in Fig. 5. Referring to this figure, a few points are worthy of note. The function $G'(\tau)$ is folded about $\tau = 0$ so that the Fourier transform result will be real and even. Filling out the pretransform array with zeros brings the array size to a power of 2 for the FFT and also increases the resolution of the transform. Passing the spectrum through the specified rectangular filter window results in the discarding of 65% of the points and performs the obvious function of eliminating low- or high-frequency noise which may be mistakenly identified as the velocity peak. Once the peak within the filter window is found a parabola is fitted to it to obtain a better estimate of the peak value. The velocity corresponding to this peak value is then the most

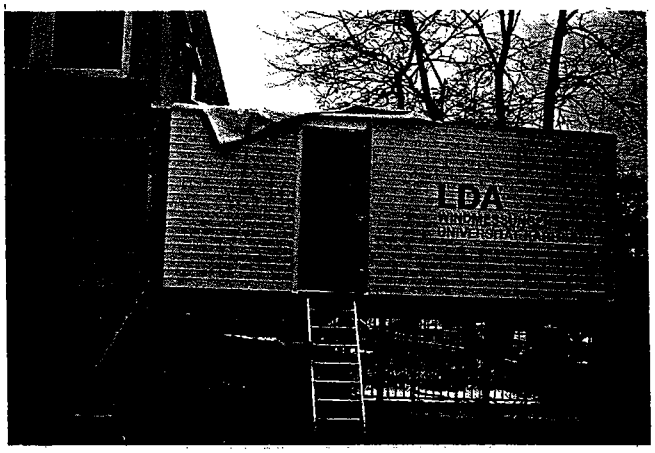

Fig. 6. Container for LDA wind velocity measurements.

for the optical components, to establish the accuracy of mechanical adjustments, to gain experience in handling the optics together with the electronics, etc. These first outdoor LDA studies of the authors led to the conclusion that successful long-time outdoor measurements require a self-contained system, see Ref. 22. A mobile measuring cabin was set up as shown in Fig. 6 and consists of a normal size container 2.5 × 2.5 × 6 m (8 × 8 × 20 ft), but with extra reinforcement to guarantee mechanical stability.

A special optical table mounted in the container supports the transmitting and receiving optics and the laser. The table can be tilted by a hydraulic lifting system, which also opens part of the roof for clearance of the outgoing beams. This arrangement allows measurements along an arc between −5 and +45° to the

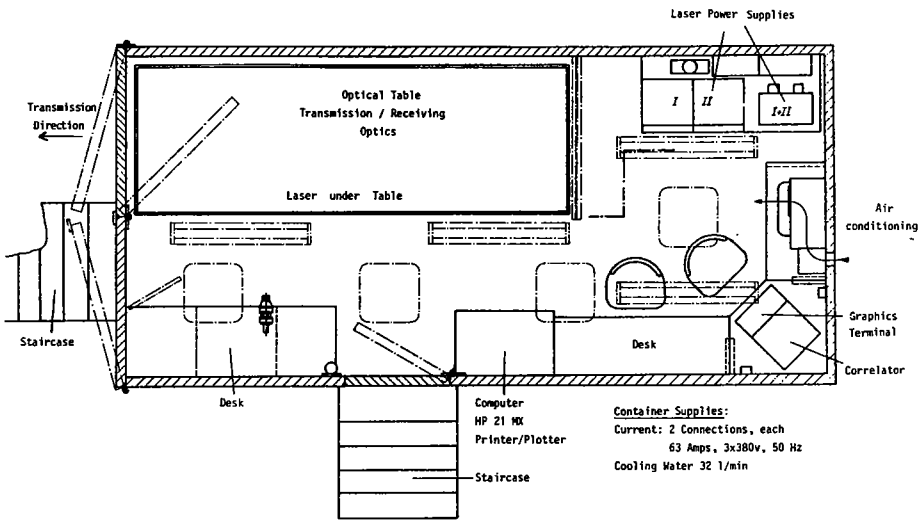

Fig. 7. Principal arrangements of container instrumentation and equipment.

probable velocity; if the velocity probability density function is symmetric, this will also be the mean value. A first-order estimate of the rms velocity $\sqrt{u'^2}$ present within the correlation time is obtained from the second moment of the parabola used to find the velocity peak (see Ref. 21). To obtain the required velocity information in the form needed to characterize the wind field subsequent off-line analysis of the stored data is carried out to generate time histories of velocities and SNR along with probability density functions. These permit mean quantities and higher-order moments of the velocity field to be computed.

IV. Laser-Doppler Anemometer for Wind Velocity Measurements

A. General Description of the Complete LDA System

Successful test measurements of wind velocities were carried out with a laboratory system on the grounds of the Universität Karlsruhe to yield information on the required system stability for long-time outdoor measurements and to gain experience on suitable materials horizontal and thus at different heights above the ground. All control units necessary for the functioning or adjustment of the LDA measuring system are also in the container permitting the operator to control the laser power, the transmitting and receiving optics, the digital correlator, and the computer for the evaluation of the signal information. The layout of all components inside the container is provided in Fig. 7. The entire system is fitted with air-conditioning and/or heating facilities to permit measurements throughout the year and in various weather conditions.

Figure 8 shows the baseplate of the optical system, consisting of an optical table with a steel honeycomb core and a 0.2- × 1.2- × 3.6-m metal skin. An additional mounting shelf supports the laser on the underside of the table. The special requirement for high laser power in the visible spectrum led to the choice of an Ar-ion laser (Spectra-Physics model 921) with a maximum continuous power output of 20 W in the green line λ = 514.5 nm. From the laser the beam is directed upward through an access hole in the table to the optical arrangement on the top surface by means of two beam-steering mirrors.

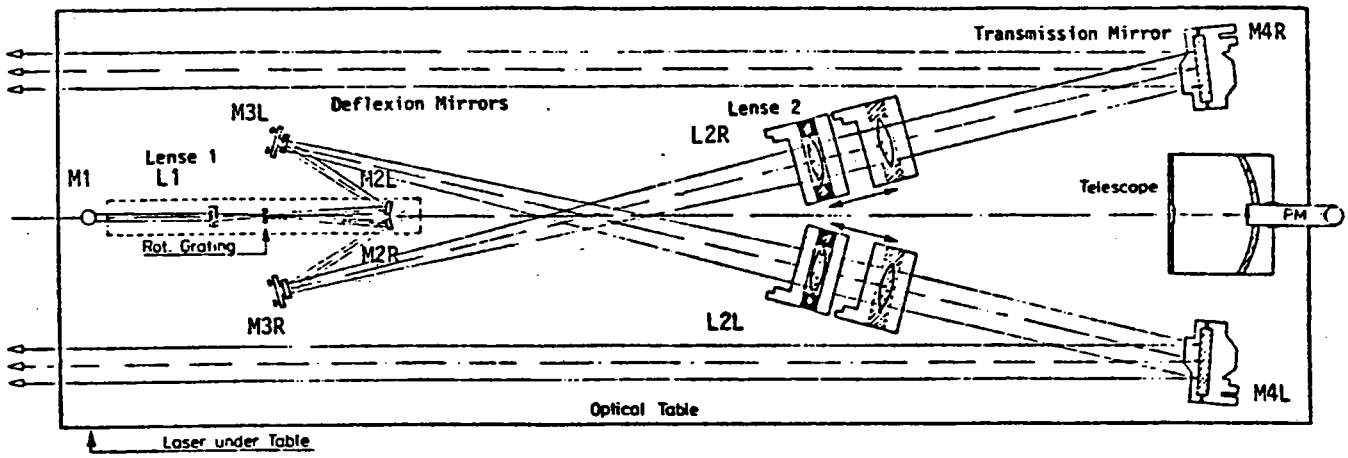

Fig. 8. Scheme of the optical system; transmission and receiving optics are shown.

Figure 8 gives a schematic view of the optical system mounted on the top surface of the baseplate. Referring to this figure, mirror $M1$ takes the beam coming from the laser under the table and guides it to a short focal length easily exchangeable lens $L1$, which focuses the beam on a rotating diffraction grating (TPD type H, with a nominal efficiency of 70%). The grating splits the incident beam into two beams and provides frequency shifting proportional to the angular velocity of the grating. The grating is a critical component of the system since all the laser power is focused in a very small beam diameter at this stage. As long as the grating is rotating, power densities as high as 56 kW/mm^2 (20 W, f = 60 mm) have produced no problems. The two beams coming from the grating are directed by mirrors $M2$ and $M3$ through focusing lenses $L2$ (f = 2250 mm, diameter = 150 mm). Transmitting mirrors $M4$ cross the beams at the desired measuring distance. The distance between $L1$ and $L2$ can be adjusted so that the focal point of the beams is also at their crossing point.

As a standard size for the measuring volume diameter a value of ~2 mm was aspired. Smaller diameters would effect a higher intensity in the measuring volume but would reduce the number of fringes in the measuring volume and would render more difficulties in crossing the two beams at long distances. The layout of the transmitting optics was made for ranges of 30–500 m. To avoid excessive loss of laser power the number of components was minimized and all optical surfaces received coatings for argon-ion-laser wavelengths. To minimize beam profile distortions within the optical system all optical surfaces were flat to $\lambda/10$ or better.

The focusing of the laser beams in the measuring volume is performed by a combination of two lenses. The first lens $L1$ focuses the laser beam onto the rotating grating and is exchangeable. Three different lenses (300, 160, and 60 mm, depending on the measuring distance) are provided to optimize the measuring volume diameter. As a function of its position in relationship to the grating, the second lens, e.g. L2L for the Ke left hand beam, of f = 2250 mm shifts the beam waist into the measuring volume. Figure 9 shows the diameter of the control volume as a function of measuring distance and of the focal length of the first lens.

For a fixed separation between the beams at the transmitting mirrors an increase in the measuring range R results in a decrease in the crossing angle 2φ between the two laser beams and therefore an increase in the fringe separation Δx. For the actual beam separation B = 0.813 m and wavelength λ = 514.5 nm the following fringe spacing can be computed:

$$\Delta x = \lambda/2 \sin\varphi \approx \frac{\lambda}{B} \cdot R = 0.633 \cdot 10^{-6} \cdot R[m]. \qquad (9)$$

In computing the velocity this fringe spacing is multiplied by f_D the inverse of the time a particle needs to cross one fringe.

Scattered light from particles in the measuring volume is collected by the receiving optics, a Schmidt-Cassegrain telescope (Celestron C14) with 355-mm clear aperture and 3910-mm focal length. The light is focused onto a 100-μm pinhole and is passed through a 1.2-nm wide 50% transmission bandpass filter λ = 514.5 nm onto a photomultiplier (EMI 9863 KB/100) chosen for its low dark count rate.

Three optical axes are defined by the two laser beams which must not only cross but also be focused at the measuring volume and the receiving optics. A total of nine stepping motors are used to control the three degrees of freedom of each axis. The elevation and azimuthal resolution of the optical mounts (mirrors $M4$ and receiving telescope) must be very high: 0.2 sec of arc corresponding to an actual linear displacement of 0.6 mm at 100 m.

The output signal of the photomultiplier is fed through to the signal processing electronics mounted in the back of the container. Details of the electronics and its functioning are provided in Sec. III. For the test measurements carried out on the grounds of the Universität Karlsruhe the beams were directed horizontally, at a height of 2.8 m, along a closed street to a small plot of grass. To prevent the two beams from continuing on into a major traffic intersection two aluminum plates mounted on a large wood panel served as beam stops. The plates were black anodized and mounted at 45° so

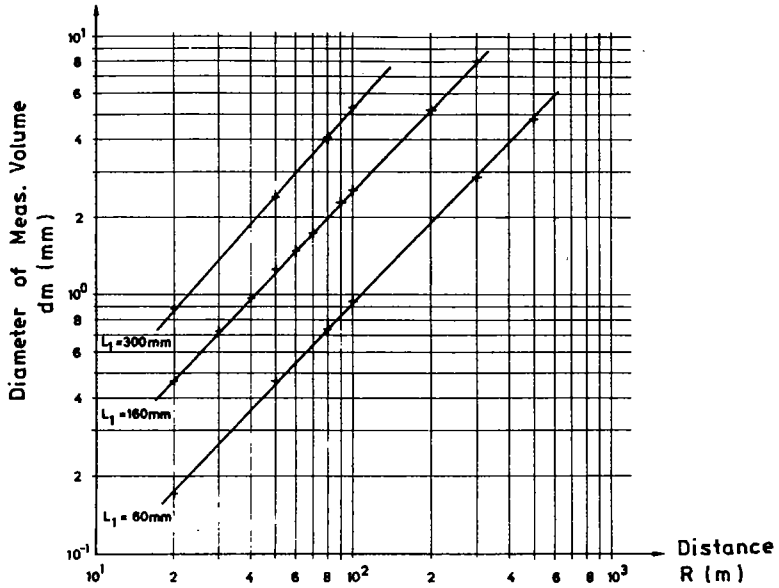

Fig. 9. Beam diameter as a function of measuring distance.

that none of the incident laser light would be scattered back into the receiving optics. Because buildings were nearby, mean velocities were low, while the relative velocity fluctuations were high. The maximum velocity for all measurements was 7 m/sec, and in most cases velocities of 2 m/sec were typical.

To compare the results of LDA measurements with those obtained with an accepted standard a sonic anemometer (Kaijo Denki model DAT-310) was employed. The sonic anemometer was positioned so that its measuring volume overlapped that of the LDA. The basis of the instrument is also the Doppler principle; the time a sound pulse needs to travel between two fixed points (in this case 0.20 m apart) is a function of the air velocity between the two points. The particular instrument used measured all three velocity components. Two, along with an electronic vector synthesizer, were used to produce a voltage linearly related to the velocity perpendicular to the LDA optical axis and in the plane of the two laser beams. The sonic instrument was compared with a Pitot tube in the SFB 80 1.5 × 1.5-m wind tunnel with good agreement. For the measurements reported herein the estimated uncertainty is ±0.1 m/sec.

During the comparative test measurements the output of the sonic anemometer was plotted on a strip chart recorder to capture all the fluctuations (0–10 Hz) and was also averaged by an integrating digital voltmeter. These voltages, proportional to velocity, were recorded by the data acquisition system to be used later for quantitative comparisons with simultaneous LDA results.

B. Wind Velocity Measurements

With the complete system described in Sec. IV.A, continuous measurements were made on the grounds of the Univesität Karlsruhe between 13 Jan. and 6 Feb. 1981, starting at 33 m and progressing to 106 m. Only the data taken toward the end of the measurement series that correspond to the longer distances are presented in this section, since measurements at smaller distances have been reported in a conference presentation, see Ref. 22.

Figure 10 shows one time series of velocity as measured at a distance of 78 m by the LDA system and the sonic anemometer. The signals follow each other quite closely. Also included for comparison purposes are probability density functions of velocities measured by the LDA system and the sonic anemometer. Cross plots of the data are provided for records taken at the same time and for the same time interval. Similar results are presented in Fig. 11 for a distance of 106 m as a further typical example of velocity records and comparative test data.

Comparative selected quantitative data are also provided in Table I. The time-averaged LDA values V(LDA) tend to be lower than the corresponding sonic data V(sonic) by ~0.15 m/sec. These differences in the mean value are also reflected in the intercept values of the regression analysis. This can be attributed to possible errors in the sonic results (uncertainty of ±0.1 m/sec) over long times or to a long-term drift in the speed of the motor driving the rotating diffraction grating. The slope and intercept given in Table I give the best transfer function in the least squares linear sense between V(sonic) and V(LDA). The slope would ideally be unity; indeed, in most cases unity does fall within the 95% confidence intervals. The correlation coefficient indicates how closely the points cluster about the regression line and expresses how well one could predict V(LDA) from a value of V(sonic). Considering the differences between the two instruments both physically, in the size of their measuring volumes, and in their sampling procedure, the correlation is considered very good.

The differences in the sampling methods between the two signals are obvious and may be another reason for the small discrepancies between LDA data and results from the sonic anemometer. The output from the sonic anemometer is a continuous low-pass filtered signal which can be sampled at fixed time intervals and integrated over various time steps. Although the LDA signal integration time was identical with that of the sonic anemometer, one set of LDA data could, in the extreme case, represent the passage of only one particle with a duration time of the order of 1 msec. This value is then taken to represent the velocity over the entire sample interval, which usually varied between 1 and 8 sec. In the other extreme, many particles may contribute to form one LDA correlogram, which will then give a more representative value of the velocity during the integration time. These differences must be considered when comparisons are made on the basis of the data provided in Table I.

In addition to computing the frequency of LDA sig-

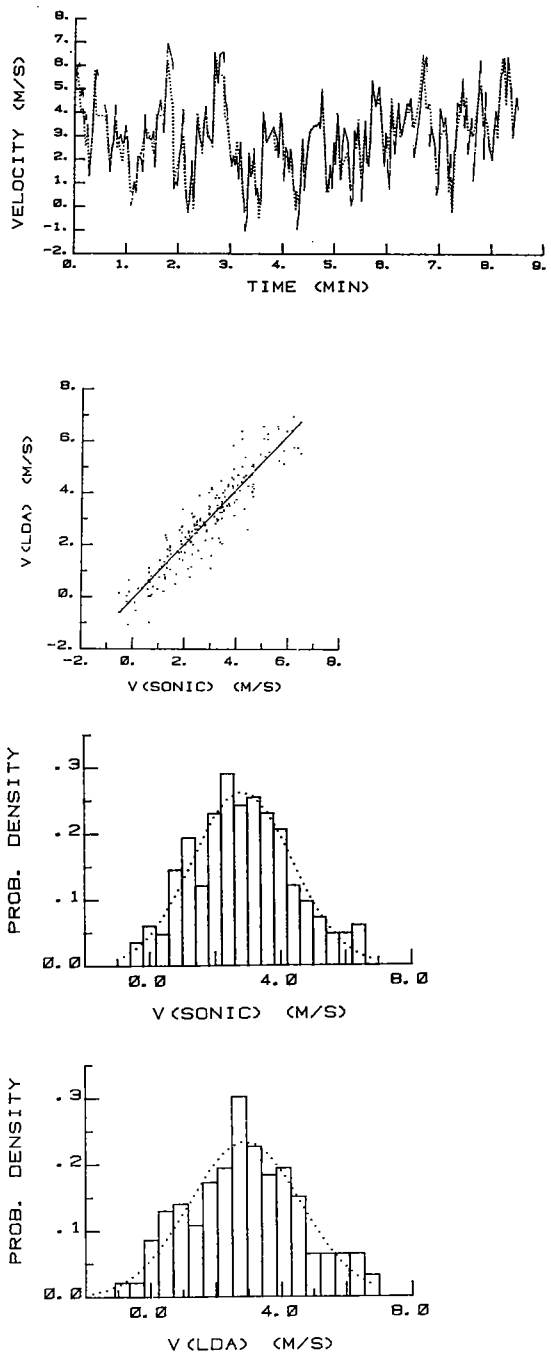

Fig. 10. Comparison of measurements: LDA-sonic method, measuring distance 78 m.

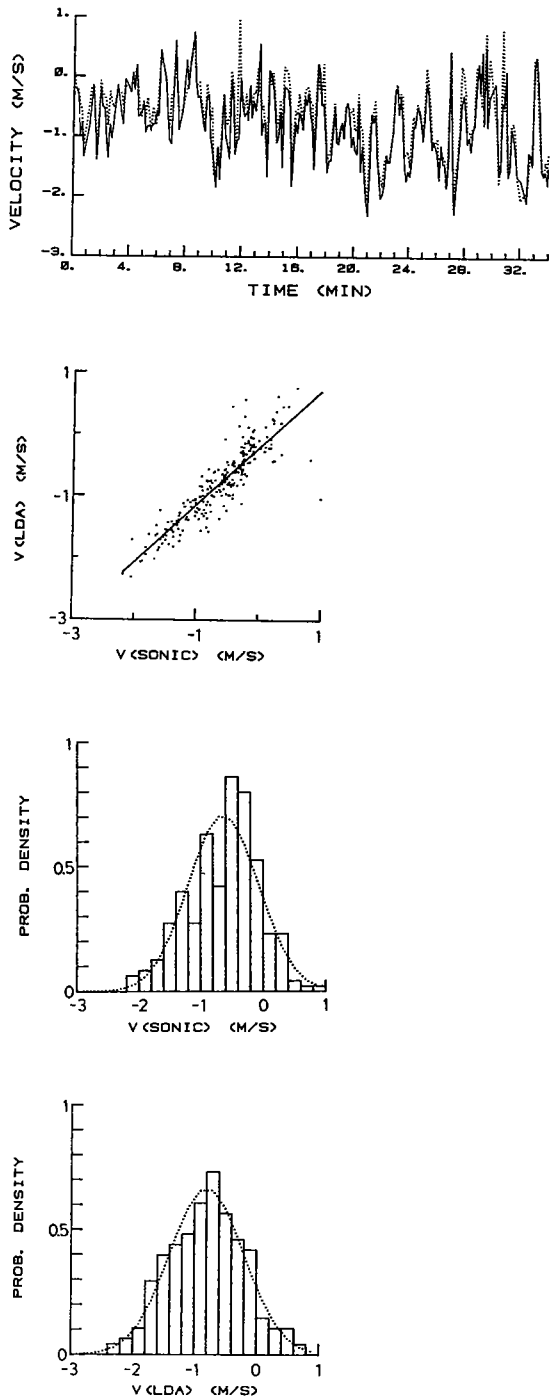

Fig. 11. Comparison of measurements: LDA-sonic method, measuring distance 106 m.

Table I. Summary of Selected Wind Records

Date Starting Time	2/1/81 05:58 h	2/3/81 08:14 h	2/5/81 05:24 h	2/5/81 08:02 h
Equipment parameters				
Range (m)	78	78	106	106
Fringe spacing (μm)	49	49	67	67
Laser power (W)	3	5	7	6.5
Sample averaging time (sec)	4.0	2.0	8.0	8.0
Length of data record (min)	17.1	8.5	17.1	34.2
Wind statistics				
$\bar{V}$ (sonic) (msec^{-1})	0.79	2.84	−0.44	−0.64
$\bar{V}$ (LDA) (msec^{-1})	0.61	2.90	−0.60	−0.80
V' (sonic) (msec^{-1})	0.56	1.52	0.59	0.57
V' (LDA) (msec^{-1})	0.57	1.70	0.60	0.60
$\overline{[(V(\text{LDA})-V(\text{sonic})]2)^{1/2}}$ (msec^{-1})	0.26	0.66	0.28	0.32
Linear regression analysis [V(sonic) = x, V(LDA) = y]				
Slope	0.960 ± 0.039	1.050 ± 0.059	0.944 ± 0.073	0.928 ± 0.06
Intercept (msec^{-1})	−0.15 ± 0.04	−0.60 ± 0.19	−0.17 ± 0.05	−0.21 ± 0.05
Correlation coefficient	0.95	0.93	0.92	0.89
SNR statistics				
$\overline{\text{SNR}}$	3.88	4.30	3.19	4.93
SNR median	3.70	3.76	3.04	4.15
SNR′	1.17	2.88	0.87	3.17
% of LDA signals, SNR > 1.5	98.8	80.5	98.4	93.4

nals from the recorded correlograms, information was also obtained on the signal-to-noise ratio (SNR) after the Fourier transform. The SNR statistics are also shown in Table I, including the fraction (in %) of LDA signals with a SNR >1.5. When this fraction of signals is less than unity, an optimal sampling frequency equivalent to a maximum average signal rate can be calculated by dividing the correlation integration time by the fraction of signals accepted. Taking the second case in Table I as an example, this frequency is 1.1 Hz. Given faster computing capability, this would be the maximum real-time data rate to be expected for the particular experimental conditions for record 2. This was the fastest record taken by the authors, and experience indicates that this may be the limit for the velocity range studied. This limit is not dependent on the system parameters but depends on the available particles and the corresponding signal quality. It is a quality that is strongly weather dependent and will also show regional variations.

Further evidence of the critical role the atmospheric particles play in LDA wind velocity measurements is presented in Figs. 12 and 13. Figure 12 shows the SNR time history corresponding to record 4 in Table I. The SNR throughout the entire time record is satisfactory, but one can see that at the time of 1 to 2 min after the record was started the SNR increased dramatically from ~1.7 to 8, indicating a change in the particles, their size, and/or their optical properties. Figure 13 shows the medium SNR as a function of laser power for two runs separated by 3 h. For the lower set of points, the medium SNR rises to ~2 at a laser power of 7 W. For the higher set of data a signal-to-noise ratio of 4 has already been reached at a laser power of 2 W. For both curves the count rates per 1-W laser power are provided as a number of pulses per second from the PM discriminator output. The factor of 12 difference between these two figures also indicates a drastic change in the particle distribution; specifically, a large number of small particles were present at the time the lower SNR values were measured, whereas for the higher SNR values the particle size distribution had a higher number of larger particles. This readily suggests that the resultant SNR of the correlograms is not a direct function of the count

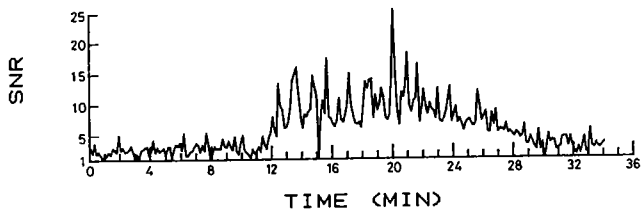

Fig. 12. SNR time history.

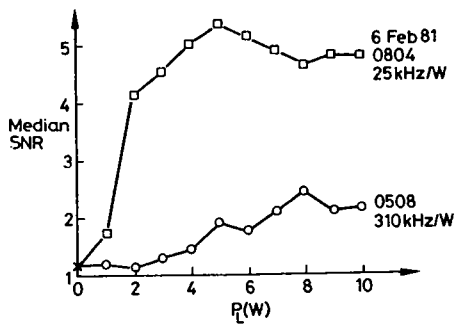

Fig. 13. Median SNR as a function of laser power.

rate of photon electron pulses per laser power recorded at the output of the photomultiplier.

During the entire measuring periods the authors were able to obtain wind velocity information at all distances over which the measurements were taken. In optimum particle conditions measurements could be taken at ~1/sec, at a distance of 106 m whereas at reduced signal quality correlograms had to be recorded up to 8 sec for each velocity record. Further tests in different weather conditions and at different spatial locations are required to draw any final conclusions on existing limits of LDA wind velocity measurements with respect to weather and regional differences.

V. Predictions of Achievable Measuring Distances

Our research on laser-Doppler systems for wind velocity measurements also aimed at finding the achievable measuring distance as a function of (a) the available laser power, (b) the parameter of the transmission and receiving optics, (c) the particle size distribution, the particle concentration, and the optical properties of the particle material, and (d) the received background radiation.

Computer programs developed by Cherdron *et al.*[17] were used to predict the achievable measuring distance and its dependence on the aforementioned influencing parameters. The reliability of these predictions was demonstrated by direct comparison with experiments carried out over distances up to 106 m.

To reduce the number of influencing parameters predictions of LDA signal properties were only performed for the optical system described in Sec. IV and for particle properties classified as maritime. In addition, zero background radiation was assumed in these predictions. It had been shown in a separate experimental study by König *et al.*[23] that background radiation to some extent only influences the integration time required for the recorded correlograms but does not prevent LDA signals from being detected. Measurements were performed with background photon rates up to values exceeding the signal photon rate by 1 order of magnitude. (These findings were obtained for measurements in which the background radiation is low enough not to saturate the entire detection system.)

The computations in Sec. II provide a limit in particle diameter, $(2r_p)_L$, above which the scattered light power yields electron pulse rates higher than the limited rate required to detect the resultant Doppler frequency. The number of particles per second that satisfy the requirement $(r_p) \geq (r_p)_L$ can be computed from the information on the particle size distribution, i.e., from the equation

$$\dot{N}_p = A \cdot U \cdot \int_{(r_p)_L}^{\infty} C(r_p) dr_p. \tag{10}$$

Using the diagrams in Fig. 3 permits the average number of successful measurements to be computed by the above formula to be of the order of 0.1–1.0/sec. This is in agreement with the experiments where the data rate for successful LDA measurements was found to be of that order. This indicates that the employed computer program yields results that are in agreement with experimental findings.

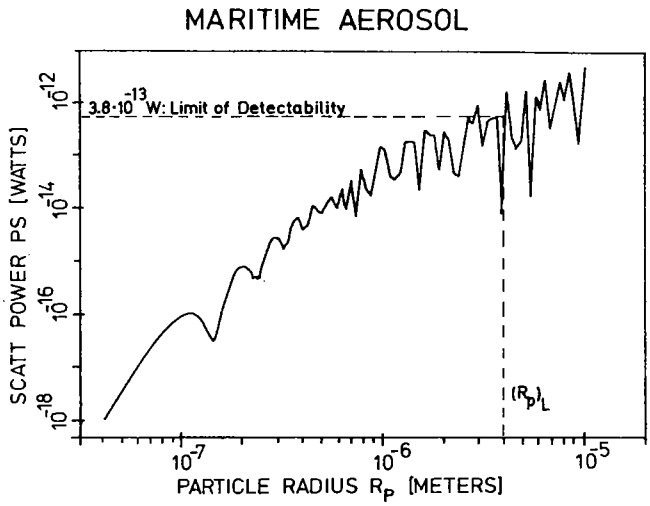

Fig. 14. Scattered light power for a measuring distance of 500 m, 10-W laser power in measuring volume.

The computations in Sec. II were repeated for distances exceeding 100 m. The measurements basically revealed that with larger distances the data rate has to be reduced drastically with the square of the measuring distance. Figure 14 shows computations for a distance of 500 m. Repeating the computations described above yields a reduced data rate by ~25 as expected. This means that at larger distances the time resolution for the flow measurements has to be reduced. Time-averaged measurements are still possible at a distance of 500 m. Larger distances do require increased laser power.

VI. Conclusions and Final Remarks

Laser-Doppler measurements of crosswind velocity components have been shown to be feasible with visible laser radiation for distances up to several hundred meters and more. Considerations of resultant light frequencies and required laser power have indicated the advantages of the visible radiation for measurements of the crosswind velocity components that are usually the cross-axial velocity components with respect to the employed LDA optical system. The axial velocity component is measured best with infrared laser radiation if these measurements are attempted with a reference-beam LDA system. The combination of dual-beam laser-Doppler systems operating with visible laser radiation and a reference-beam laser-Doppler system operating with infrared lasers is suggested for three component measurements.

Specially developed computer programs to predict the performance of laser-Doppler systems when employed for measurements of atmospheric flows over large distances revealed the feasibility of such systems for quantitative studies of wind fields. Theoretical knowledge of the design of the optics and experimentally gained information on the performance of electronic units for photon resolved signal detection, per-

mitted the design of a complete, containerized system. This system was employed for verification experiments at distances up to 106 m. Comparisons with wind velocity measurements obtained by ultrasonic flowmeters showed good agreement with corresponding LDA results.

The extension of the studies permitted predictions of achievable measuring distances with available laser power; 500 m and more should be possible. Larger distances require development of new lasers with higher power outputs. In addition, in some of the foreseeable applications more efficient lasers are necessary than the Ar-ion laser employed in the present experiments.

Before production of practical LDA systems for wind velocity measurements our research and development will be extended to yield (1) more compact optical systems incorporating highly efficient laser light sources; (2) a higher degree of automation of the electronic system and faster data acquisition; and (3) more information on the limitations of the system with respect to weather conditions and regional differences in aerosol distributions.

The continuation of this work will ensure that 3-D LDA systems for wind velocity measurements over large distances will be available in the near future.

The present work is based on basic research and development in laser-Doppler anemometry and its application to fluid flow measurements financed by the Deutsche Forschungsgemeinschaft as part of the research program of the Sonderforschungsbereich 80 at the Universität Karlsruhe, Federal Republic of Germany. The specific work on laser-Doppler wind velocity measurements was financed initially by the Bundesministerium der Verteidigung, RüFo-3, and was continued by the Bundesamt für Wehrtechnik und Beschaffung, FE-IV-6. The authors gratefully acknowledge the support of their work.

References

1. W. C. Cliff and R. M. Huffacker, "Application of a Single Laser-Doppler System to the Measurements of Atmospheric Winds," Marshall Space Flight Center, Alabama, NASA Tech. Memo. X64891 (1974).
2. W. R. M. Pomeroy, J. M. Vaughan, and D. V. Willetts, "Performance Study of an Acousto-Optic Frequency Shifter in a CO_2-Laser Velocimeter," RSRE, Great Malvern, Worcs., U.K., to be published.
3. S. Karaki, "A Comparison of a Coaxial Focused Laser-Doppler System in Atmospheric Measurements," NASA Contract. Rep. 124355 (1972).
4. T. R. Lawrence *et al.*, Rev. Sci. Instrum. **43,** 512 (1972).
5. A. J. Hughes and E. R. Pike, Appl. Opt. **12,** 597 (1973).
6. E. W. Eloranta *et al.*, J. Appl. Meteorol. **14,** 1485 (1975).
7. R. L. Schwiesow, R. E. Cupp, M. J. Post, and R. F. Calfee, Appl. Opt. **16,** 1145 (1977).
8. M. J. Post *et al.*, J. Appl. Meteorol. **17,** 1179 (1978).
9. J. M. Vaughan, "Remote Measurements in the Atmosphere Using Laser-Doppler Methods," Plenary paper presented at LASER 79, Munich (1979).
10. C. A. DiMarzio and J.W. Bilbro, "An Airborne Doppler Lidar," in *Proceedings, NASA Heterodyne Systems Technology Conference, Williamsburg* (1980).
11. W. M. Farmer and D. B. Brayton, Appl. Opt. **10,** 2319 (1971).
12. P. J. Bourke and C. G. Brown, J. Opt. Laser Technol. 23 (1971).
13. K. G. Bartlett and C. Y. She, Appl. Opt. **15,** 1980 (1976).
14. L. Lading, A. S. Jensen, C. Fog, and H. Andersen, Appl. Opt. **17,** 1486 (1978).
15. W. L. Eberhard and R. M. Schotland, Appl. Opt. **19,** 2967 (1980).
16. L. Danielsson, "Experiments with Laser-Fringe Velocity Measurements over Large Distances in the Atmosphere," in *Proceedings, Fourth International Conference on Photon Correlation Techniques, Stanford* (Joint Institute for Aeronautics and Acoustics, Stanford U., Calif., 1980), pp. 4/1–4/12.
17. W. Cherdron, F. Durst, and G. Richter, *Computer Programs to Predict the Properties of Scattered Laser Radiation, SFB 80/TM/121* (U. Karlsruhe, Germany, 1978).
18. G. Mie, Ann. Phys. (Leipzig) **25,** 377 (1908).
19. J. Abele, "Neuere Aerosolmessungen im Bereich 0.15-30μm unter besonderer Berücksichtigung optischer Effekte," Tübingen, report FFO 1980/62.
20. E. R. Pike, *Photon Correlation Velocimetry and Spectroscopy* (Plenum, New York, 1977), pp. 246–343.
21. J. B. Abbiss, Phys. Scr. **19,** 388 (1979).
22. F. Durst, B. Howe, and G. Richter, "Long Range LDA Wind Velocity Measurements Using Visible Laser Radiation," in *Proceedings, Fourth International Conference on Photon Correlation Techniques, Stanford* (Joint Institute for Aeronautics and Acoustics, Stanford U., Calif. 1980), pp. 3/1–3/13.
23. M. König, H. J. Pfeifer, E. Sommer, and B. Koch, "Photonkorrelation als Auswerteverfahren der Laseranemometrie bei gepulstem Laserbetrieb und starkem Störlicht," Deutsch-Französisches Forschungsinstitut Saint-Louis, ISL report 505/78 (1978).